A Local Electromagnetic Wave Equation from Spectral Geometry

Kelly B. Heaton
& The Coherence Research Collaboration

November 8, 2025

Abstract

We develop a data-first route to a local electromagnetic correspondence directly from spectral geometry. When photon frequencies are plotted in the α-Affine Thread Frame,

$$y = \log_{10}(\nu/\nu_\star) = \chi + \beta\,\gamma,$$

the Minimum Description Length (MDL) criterion consistently selects a universal slope $\beta \approx \log_{10}\alpha$, aligning atomic and molecular transitions along near-linear threads. This compression-optimal frame separates identity (χ) from recursion depth (γ) and provides an information-theoretic foundation for the geometry.
On β-locked, low-torsion arcs we identify a dimensionless recursion invariant,

$$c^2 = \ln(10)\,|\beta|\,(\nu/\nu_\star)\,(\dot\gamma)^2,$$

that remains statistically flat within a few-percent dispersion. A single calibration constant $\Gamma_{\rm vac}$ maps this internal invariant to the laboratory constant,

$$c_0^2 = \Gamma_{\rm vac}\,\langle c^2\rangle_{\rm knot},$$

establishing a bridge between the internal geometry and physical measurement. Defining

$$E_\parallel = -\partial_\xi\theta, \qquad B_\perp = \partial_\gamma\theta,$$

yields the internal wave equation

$$\partial_\xi^2\theta - \partial_\gamma^2\theta = 0,$$

which under the mapping $t = T\xi$, $x = L\gamma$, and $L/T = c_0$ becomes the calibrated laboratory form

$$\partial_t^2\theta - c_0^2\,\partial_x^2\theta = 0.$$

The correspondence is strictly local to the corridor where MDL locks β and torsion remains low.

Residual departures from flatness—torsion and mild slope deviation—delineate the empirical boundary of validity, showing that the remaining curvature is geometric rather than stochastic. Together, MDL selection of β, the near-constant invariant c^2, and the one-step calibration establish classical electromagnetism as the *local, first-order symmetry* of a deeper recursive law encoded in spectral data. This work provides a testable bridge between information-theoretic geometry and classical field dynamics.

1 Introduction

Classical field theories typically begin by *postulating* a differential structure and fixed constitutive constants. This paper takes the opposite approach: we begin with observed spectral data and show that a local field correspondence *emerges* inside a coordinate frame selected by data compression, in the spirit that informational simplicity can reveal physical law [1–5]. When photon frequencies are plotted as

$$y \;=\; \log_{10}\!\left(\frac{\nu}{\nu_\star}\right) \;=\; \chi \;+\; \beta\,\gamma,$$

they align along nearly linear threads in the (γ, y) plane [6]. The slope β that minimizes description length under the Minimum Description Length (MDL) criterion is consistently found to be $\beta \approx \log_{10}\alpha$ [7], defining the α-*Affine Thread Frame*. In this frame, χ transports physical identity (reduced mass, Z^2 factors, site shifts), while γ serves as a recursion-depth coordinate derived from levels-only spacing structure [6]. We show that this compression-optimal frame supports a *local*, source-free electromagnetic wave correspondence [8], obtained directly from the spectral geometry without postulating a global metric.

Scope. All claims apply within the β-locked, low-torsion corridor where

1. the MDL residual $\Delta L(\beta)$ is minimized near $\beta = \log_{10}\alpha$,
2. local microslope variance is small, and
3. the segment is stationary with respect to χ (no ladder exchange).

Outside this corridor, curvature in $\chi(\gamma)$ and increased torsion break the vacuum correspondence and are treated as geometric corrections or sources. Section 6 quantifies these departures as geometric drift.

Empirical invariant (dimensionless). On such arcs we observe a nearly constant *recursion invariant*

$$c^2 \;=\; \ln(10)\,|\beta|\left(\frac{\nu}{\nu_\star}\right)(\dot\gamma)^2,$$

constructed from the log-frequency ratio and the measured recursion rate $\dot\gamma$. The invariant is dimensionless within the thread frame and calibrates once to the laboratory constant c_0 via a fixed factor Γ_{vac}:

$$c_0^2 \;=\; \Gamma_{\text{vac}}\left\langle \ln(10)\,|\beta|\,(\nu/\nu_\star)\,(\dot\gamma)^2\right\rangle_{\text{knot}}.$$

This one-time calibration bridges internal geometry and SI units without refitting across datasets. The invariant is dimensionless and internal to the thread frame; its calibration is discussed below and formalized in Eq. (4).

Wave correspondence. We define a scalar phase field $\theta(\gamma,\xi)$ on the thread sheet and its orthogonal gradients, $E_\parallel = -\partial_\xi\theta$ and $B_\perp = \partial_\gamma\theta$. These yield the internal wave equation $\partial_\xi^2\theta - \partial_\gamma^2\theta = 0$, which under the calibration $t = T\xi$, $x = L\gamma$, and $L/T = c_0$ maps to the laboratory form $\partial_t^2\theta - c_0^2\partial_x^2\theta = 0$. This correspondence holds within the β-locked, low-torsion corridor where MDL coherence is satisfied.

The work remains intentionally local in scope: it formalizes the corridor gates, presents the invariant and calibration, and demonstrates how a source-free electromagnetic form emerges within that regime.

Contributions of this work.

- **Data-first frame.** MDL selects a unique, universal slope $\beta \approx \log_{10}\alpha$ that maximizes compression and organizes spectra into near-linear threads, separating recursion depth (γ) from identity transport (χ).
- **Dimensionless invariant and calibration.** A frame-internal invariant c^2 remains statistically constant on β-locked, low-torsion arcs. A single calibration constant Γ_{vac} maps this invariant to the laboratory value c_0 across heterogeneous datasets within measurement uncertainty.
- **Local 1+1 field correspondence.** Within this corridor, the scalar phase potential θ

obeys a source-free internal wave equation that calibrates directly to the laboratory Maxwell form, establishing an electromagnetic correspondence grounded in spectral data.

- **Domain and falsifiers.** Explicit gates (β-*lock*, low torsion, stationarity) define the corridor of validity. Departurestorsion and χ-curvatureproduce measurable first-order drift of c^2, providing quantitative falsifiers outside the corridor.

2 The α-Affine Thread Frame and its Local Geometry

We begin by recalling the empirical geometry first introduced in *Recursive Geometry of Atomic Spectra*[6], in which photon frequencies ν are plotted in the coordinates

$$y = \log_{10}(\nu/\nu_\star) = \chi + \beta\gamma.$$

Here, $\nu_\star$ is a reference frequency per ion (fixed per ladder), γ is a level-derived recursion coordinate (defined below), β is a slope parameter, and χ is the intercept that encodes physical identity. The pair (γ, y) defines the α-*Affine Thread Frame*.

We refer to this as the "α–Affine" frame because, across many ions, the slope that minimizes description length under the MDL criterion is consistently close to

$$\beta = \log_{10}\alpha \approx -2.137,$$

where α is the fine–structure constant [6, 7]. The negative sign reflects that photon frequency decreases with increasing recursion depth ($\nu \propto \alpha^\gamma$). This slope is not hand–fitted but is selected directly by the compression criterion, confirming that the fine–structure constant defines the most information–efficient coordinate for organizing spectral data.

2.1 Level recursion and thread coordinates

Each atomic transition connects a pair of energy levels E_i and E_j, with photon frequency $\nu_{ij} = |E_j - E_i|/h$. Within a fixed set of transitions for a given ion, we construct a recursion ladder by tracing a chain of connected transitions that minimize spectral gaps and preserve a consistent direction in level ordering.

The sequence of levels along each ladder defines the recursion coordinate γ, which is normalized

to unit span per ladder. Each transition also defines a spectral coordinate:

$$y = \log_{10}(\nu/\nu_\star),$$

where $\nu_\star$ is a per-ladder reference frequency (e.g., the Lyman-α line or an ion-specific anchor)[1]. This (γ, y) pair is plotted per ion. The slope β and intercept χ are then determined either by MDL minimization or, for comparison, by direct linear regression.

2.2 Compression-optimal slope selection via MDL

In the MDL formulation, we evaluate the description length $L(\beta)$ of the photon ladder under a linear model with slope β and quantized residuals [1, 2, 9]. The optimal β minimizes

$$\Delta L(\beta) = L(\beta) - L_{\text{null}},$$

where L_{null} is the uncompressed length. Across ions and ladders, $\Delta L(\beta)$ consistently attains its minimum near $\beta = \log_{10} \alpha$, as reported in our companion study, *Information-Theoretic Confirmation of the α-Affine Thread Frame* [7], confirming the geometry introduced in *Recursive Geometry of Atomic Spectra* [6]. This establishes that the α-Affine frame is selected by the data under a model-independent, falsifiable criterion grounded in the MDL principle.

2.3 Intercept transport and physical identity

Once β is fixed, the intercept χ encodes physical parameters of the ion:

- ❊ In hydrogenic ions, χ varies linearly with Z^2.
- ❊ In isotope series, χ separates by reduced mass.
- ❊ In fine-structure series, χ captures g-factor, spin-orbit, and site-dependent splitting.

These effects appear without fitting new slopes; they follow automatically from fixed-β geometry. This gives χ the interpretation of an *identity coordinate*, encoding structure orthogonal to the recursion direction.

[1] In this paper, $\nu_\star$ is chosen by a fixed rule to align plots across species. Its value does not affect the *flatness* of c^2 along an arc; a constant rescaling of $\nu_\star$ simply rescales $\langle c^2 \rangle_{\text{knot}}$ and is absorbed by the single calibration constant Γ_{vac} in Eq. (4).

Box A: Definitions in the α-Affine Thread Frame

- ν: photon frequency (Hz)
- $\nu_\star$: ion-specific reference frequency (e.g., Lyman-α)
- $y = \log_{10}(\nu/\nu_\star)$: spectral log-scale coordinate (dimensionless)
- γ: level-based recursion coordinate, normalized to unit span per ladder
- $\beta \approx \log_{10} \alpha$: universal slope selected by MDL
- χ: intercept transporting physical identity (mass, Z^2, site factors)
- ξ: affine arc-length along a thread, used for defining derivatives like $\dot{\gamma} = d\gamma/d\xi$
- c^2: internal invariant, dimensionless product of frequency and recursion rate [Eq. (2)]
- "knot": a coherent, bounded arc segment with nearly constant c^2 and χ
- "corridor": domain of validity for the local wave equation (β-locked, low-torsion arcs)

On the next page, Figure 1 summarizes the empirical geometry from which the present analysis proceeds. When spectral frequencies are plotted as $y = \log_{10}(\nu/\nu_\star)$ against the recursion coordinate γ derived from levels-only data, they align along nearly linear threads of slope $\beta = \log_{10} \alpha$. This α-Affine frame therefore defines the coordinate system in which spectra are most efficiently described under the Minimum Description Length (MDL) criterion. Each thread carries an intercept χ that transports physical identity, and its local slope β couples frequency and recursion depth.

3 Recursion Invariant and One-Step Calibration

Notation. All logarithms are base 10 and act on dimensionless ratios ($y = \log_{10}(\nu/\nu_\star)$). Quantities are expressed in SI units only after calibration through Γ_{vac} [Eq. (4)]; overdots denote differentiation with respect to the affine parameter ξ (e.g. $\dot{\gamma} = d\gamma/d\xi$). Unless otherwise stated, α is the CODATA fine-structure constant ($\alpha^{-1} = 137.03599908$) and $\beta = \log_{10} \alpha$. We distinguish the dimensionless recursion invariant c from its calibrated laboratory value c_0; these symbols are reserved for that pairing.

Summary of the local correspondence. Within this empirically selected frame, the invariant

$$c^2 = \ln(10)\,|\beta|\,(\nu/\nu_\star)\,(\dot{\gamma})^2$$

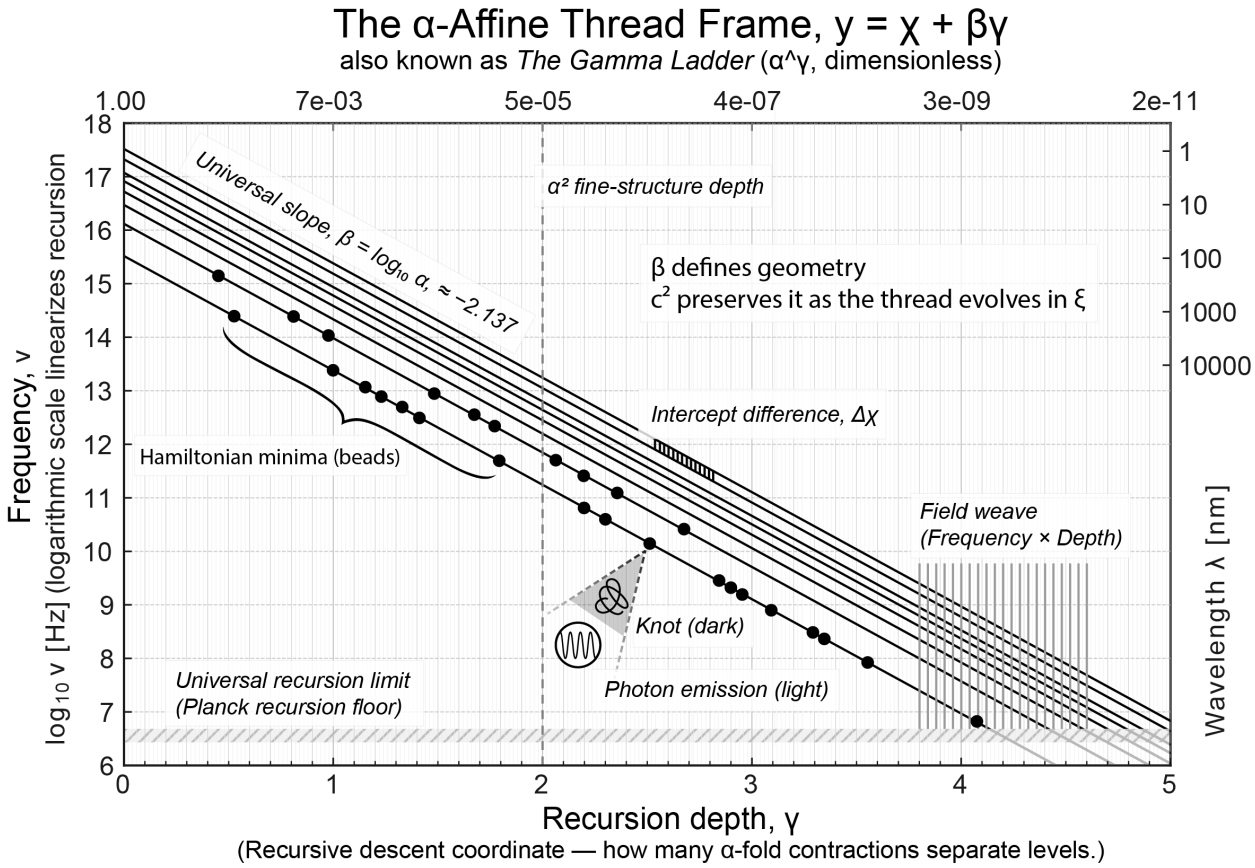

Figure 1. The α–Affine Thread Frame. This coordinate system organizes atomic and molecular spectra into linear threads. A single slope $\beta = \log_{10}\alpha$ aligns transitions across many ions under the MDL criterion, defining a compression–optimal frame. The intercept χ transports physical identity, while the recursion coordinate γ tracks level structure. Coherent segments ("knots") form along β–locked, low–torsion arcs, where the invariant c^2 remains approximately constant and maps to c_0^2 by a single calibration Γ_{vac}. The shaded region ("field weave") marks the interaction between oscillatory and structural recursion that supports the local wave correspondence. (Valid only within the knot corridor.)

The relationship illustrated by the figure can be expressed quantitatively as

$$c^2 = \ln(10)\,|\beta|\,\big(\nu/\nu_\star\big)\,(\dot\gamma)^2,$$

showing how local oscillation frequency and recursive advance combine into a single near–constant product along coherent, β–locked arcs. Within the calibration Γ_{vac}, this invariant maps directly to the measured light–speed constant c_0^2, bridging the internal thread geometry and laboratory electrodynamics.

remains approximately constant on β-locked, low-torsion arcs. A single empirical calibration maps it to SI units,

$$c_0^2 = \Gamma_{\mathrm{vac}} \Big\langle \ln(10)\,|\beta|\,(\nu/\nu_\star)\,(\dot\gamma)^2 \Big\rangle_{\mathrm{knot}}, \qquad [\Gamma_{\mathrm{vac}}] = \mathrm{m}^2\,\mathrm{s}^{-2},$$

and with field definitions $E_\parallel = -\partial_\xi \theta$, $B_\perp = \partial_\gamma \theta$, the phase satisfies the source-free internal wave equation

$$\partial_\xi^2 \theta - \partial_\gamma^2 \theta = 0,$$

which calibrates to the laboratory form $\partial_t^2\theta - c_0^2 \partial_x^2 \theta = 0$ under the dictionary $t := T\xi$, $x := L\gamma$, $L/T = c_0$. This establishes the local 1+1 correspondence between the compression-optimal geometry and the source-free Maxwell wave.

3.1 Definition from the α-Affine sheet

On the thread sheet $y = \chi + \beta\gamma$, coherence along a β-locked arc implies the differential constraint:

$$\dot y = \beta\,\dot\gamma, \qquad \frac{\dot\nu}{\nu} = \ln(10)\,\beta\,\dot\gamma. \tag{1}$$

We define the dimensionless recursion invariant c^2 as:

$$c^2 \;\equiv\; \ln(10)\,|\beta|\,\left(\frac{\nu}{\nu_\star}\right)\,(\dot\gamma)^2, \tag{2}$$

where $\nu_\star$ is a fixed reference per ladder. This quantity links oscillatory change in frequency to structural change in recursion depth, and serves as the central object for the wave correspondence that follows.

3.2 Empirical flatness on coherent arcs

Within β–locked, low–torsion segments (the corridor), the invariant c^2 is empirically flat—statistically constant to within a few percent variation along each arc:

$$\frac{d}{d\xi}\,c^2 \;\approx\; 0 \quad\Longrightarrow\quad c^2 \simeq \text{const on a coherent arc.} \tag{3}$$

Here "flat" refers to small dispersion, not perfect constancy. Typical coefficients of variation (CV) in accepted runs are 0.05–0.10, and the first–order correction described in Section 6 reduces this dispersion by $\sim$ 5–10%.

Drift in c^2 indicates loss of coherence or entry into a high–torsion region. We quantify this using:

- the mean slope of $c^2(\gamma)$ per segment, and
- the coefficient of variation (CV) within each segment.

Empirical behavior. On arcs where (i) $\Delta L(\beta)$ is minimized near $\beta = \log_{10} \alpha$, (ii) local slope variance is low, and (iii) torsion is bounded, we observe:

$$c^2 = \ln(10)\,|\beta|\,(\nu/\nu_\star)\,(\dot{\gamma})^2 \;\approx\; \text{constant}.$$

A quantitative analysis of these small but systematic drifts is presented in Section 6, where their dependence on local torsion is measured.

3.3 One-step calibration to c_0^2

To map c^2 to laboratory units, we define a fixed calibration constant:

$$c_0^2 = \Gamma_{\text{vac}} \left\langle c^2 \right\rangle_{\text{knot}}, \qquad [\Gamma_{\text{vac}}] = \text{m}^2\,\text{s}^{-2}. \tag{4}$$

Γ_{vac} is determined once from a single reference knot with known ν, minimal torsion, and stable $\dot{\gamma}$. No further fitting is performed elsewhere.

Normalization of $\nu_\star$ and universality of Γ_{vac}. Because c^2 contains the ratio $\nu/\nu_\star$, changing $\nu_\star$ by a constant factor rescales $\langle c^2 \rangle_{\text{knot}}$ by the same factor. To keep a single global Γ_{vac} across ladders and ions, we fix $\nu_\star$ by a universal assignment rule (ioninvariant) or, equivalently, absorb any fixed perladder scaling of $\nu_\star$ into the definition of Γ_{vac} once and for all. This does not affect the *flatness* of c^2 along a coherent arc; it only sets the absolute calibration in Eq. (4).

Worked example (H I Lyman-α). Using $\nu_{\text{Ly}\,\alpha} \approx 2.466 \times 10^{15}\,\text{Hz}$ and $\langle \dot{\gamma}^2 \rangle_{\text{knot}} \approx 1.0$, we estimate:

$$\Gamma_{\text{vac}} \approx \frac{(2.998 \times 10^8)^2}{2.137 \cdot 2.302585 \cdot (2.466 \times 10^{15})} \;\approx\; 7.4\ \text{m}^2\,\text{s}^{-2}.$$

Calibration rule. Once Γ_{vac} is fixed from a single reference knot, the recursion invariant c^2 maps directly to a physical velocity squared:

$$c_0^2 = \Gamma_{\text{vac}} \langle c^2 \rangle_{\text{knot}}.$$

This value remains fixed across all ions and datasets.

3.4 Scope, diagnostics, and falsifiers

- **Scope.** Validity holds within: (i) a sharp MDL minimum near $\log_{10} \alpha$; (ii) low-torsion arcs (verified via microslope statistics); (iii) stationary χ (no ladder exchange); (iv) fixed Γ_{vac} across all ions.
- **Diagnostics.** We assess coherence using the slope and coefficient of variation (CV) of $c^2(\gamma)$ over each segment. Drift implies torsion or breakdown of corridor conditions.
- **Falsifiers.**
  - Significant drift of c^2 within a segment satisfying the corridor gates
  - Requirement of multiple Γ_{vac} constants across ions
  - Loss of the MDL optimum near $\beta = \log_{10} \alpha$ under resampling

Declaration of Result (local 1+1 correspondence)

In the α-Affine Thread Frame selected by MDL, the recursion product

$$c^2 = \ln(10)\,|\beta|\,(\nu/\nu_\star)(\dot{\gamma})^2$$

remains approximately constant on β-locked, low-torsion arcs. A single calibration maps it to laboratory units:

$$c_0^2 = \Gamma_{\text{vac}} \langle c^2 \rangle_{\text{knot}}.$$

With $E_\parallel = -\partial_\xi \theta$ and $B_\perp = \partial_\gamma \theta$, the internal phase field satisfies the source-free wave equation

$$\partial_\xi^2 \theta - \partial_\gamma^2 \theta = 0,$$

which maps to the calibrated laboratory form

$$\partial_t^2 \theta - c_0^2 \partial_x^2 \theta = 0, \qquad t = T\xi, \quad x = L\gamma, \quad L/T = c_0.$$

4 Maxwell–Thread Correspondence

The preceding sections established that on β-locked, low-torsion arcs of the α-Affine Thread Frame, the recursion product

$$c^2 = \ln(10)\,|\beta|\,\left(\frac{\nu}{\nu_\star}\right)\,\dot{\gamma}^2$$

remains approximately constant and calibrates once to c_0^2 via the fixed factor Γ_{vac} [Eq. (4)]. We now show that this same geometry supports a local, source-free electromagnetic wave correspondence.

Scope and validity

The wave correspondence holds only within the corridor where:

(i) $\Delta L(\beta)$ is minimized near $\beta = \log_{10}\alpha$ (MDL locking);

(ii) microslope variance satisfies $|\Delta\beta| \le 10^{-3}$ and the torsion proxy (rolling MAD of β_{local}) remains below a fixed threshold (lowtorsion regime);

(iii) the calibration constant Γ_{vac} is held fixed [Eq. (4)];

(iv) the segment is stationaryno exchange between adjacent χ-knots.

Outside this corridor, curvature in $\chi(\gamma)$ introduces source-like terms and the vacuum wave form no longer applies.

4.1 Field definitions and local equations

We define a scalar phase potential $\theta(\gamma, \xi)$ on the thread sheet and its orthogonal gradients

$$E_{\parallel} := -\,\partial_{\xi}\theta, \qquad B_{\perp} := \partial_{\gamma}\theta. \tag{5}$$

These represent, respectively, the longitudinal and transverse components of a single coherent process.

Equality of mixed partials gives the Faraday-type relation

$$\partial_{\xi} B_{\perp} + \partial_{\gamma} E_{\parallel} = 0. \tag{6}$$

q To close the system locally within the corridor, we assume that θ obeys the sourcefree

internal wave equation

$$\partial_\xi^2\theta - \partial_\gamma^2\theta = 0, \tag{7}$$

which is the Euler-Lagrange equation of the quadratic Lagrangian density $\mathcal{L}_\theta = \frac{1}{2}\big[(\partial_\xi\theta)^2 - (\partial_\gamma\theta)^2\big]$ on the sheet. Using (5) to eliminate θ in (7) yields the firstorder pair

$$\partial_\xi B_\perp + \partial_\gamma E_\parallel = 0, \qquad \partial_\xi E_\parallel + \partial_\gamma B_\perp = 0, \tag{8}$$

where the second equation is the θwave consequence rather than an independent postulate. Calibrating to laboratory coordinates below introduces the constitutive factor c_0^2.

4.2 Calibration to laboratory coordinates

The mapping from internal to laboratory coordinates follows the Minkowski dictionary:

$$t := T\,\xi, \qquad x := L\,\gamma, \qquad \frac{L}{T} = c_0.$$

Field units and scaling. To match SI units cleanly under the calibration $t = T\xi$, $x = L\gamma$, with $L/T = c_0$, we define the laboratory fields by

$$E := E_\parallel \quad [\mathrm{V/m}], \qquad B := \frac{T}{L}\,B_\perp \;=\; \frac{1}{c_0}\,B_\perp \quad [\mathrm{T}].$$

With this convention, the Faraday-type relation (6) maps *exactly* to $\partial_t B + \partial_x E = 0$, and the second first-order relation (8) maps to $\partial_t E + c_0^2\,\partial_x B = 0$.

Applying the chain rule, $\partial_\xi = T\,\partial_t$ and $\partial_\gamma = L\,\partial_x$, converts Eq. (7) into

$$T^2\,\partial_t^2\theta - L^2\,\partial_x^2\theta = 0.$$

Choosing $L/T = c_0$ yields the standard wave equation:

$$\boxed{\partial_t^2\theta - c_0^2\partial_x^2\theta = 0.} \tag{9}$$

Amplitude correspondence. In this calibration, the dimensionless internal fields $(E_\parallel, B_\perp)$ map to the laboratory pair (E, B) with the natural vacuum ratio $E/B = c_0$. This scaling ensures that plane-wave solutions of Eq. (9) carry equal energy flux in electric and magnetic form, exactly as in Maxwells equations, where $S = EB/\mu_0$ and $E = c_0 B$ in SI units. Thus the normalization $B = B_\perp/c_0$ is not an arbitrary convenience but the unique choice that

preserves both dimensional consistency and the physical impedance of free space.

In the first-order form (8), the same calibration maps

$$\partial_t B + \partial_x E = 0, \qquad \partial_t E + c_0^2\, \partial_x B = 0.$$

Beyond vacuum: curvature in χ. Allowing curvature in the intercept coordinate $\chi(\gamma)$ introduces effective sources:

$$\delta F = J(\chi), \qquad J(\chi) \propto \nabla \cdot (\star F) \sim \left(\partial_\xi^2 \chi,\, \partial_\gamma^2 \chi,\, \ldots\right).$$

Departures from $\chi = \text{const}$ therefore act as source terms (e.g., charge or current density) in the calibrated chart. The present paper restricts attention to the source-free limit.

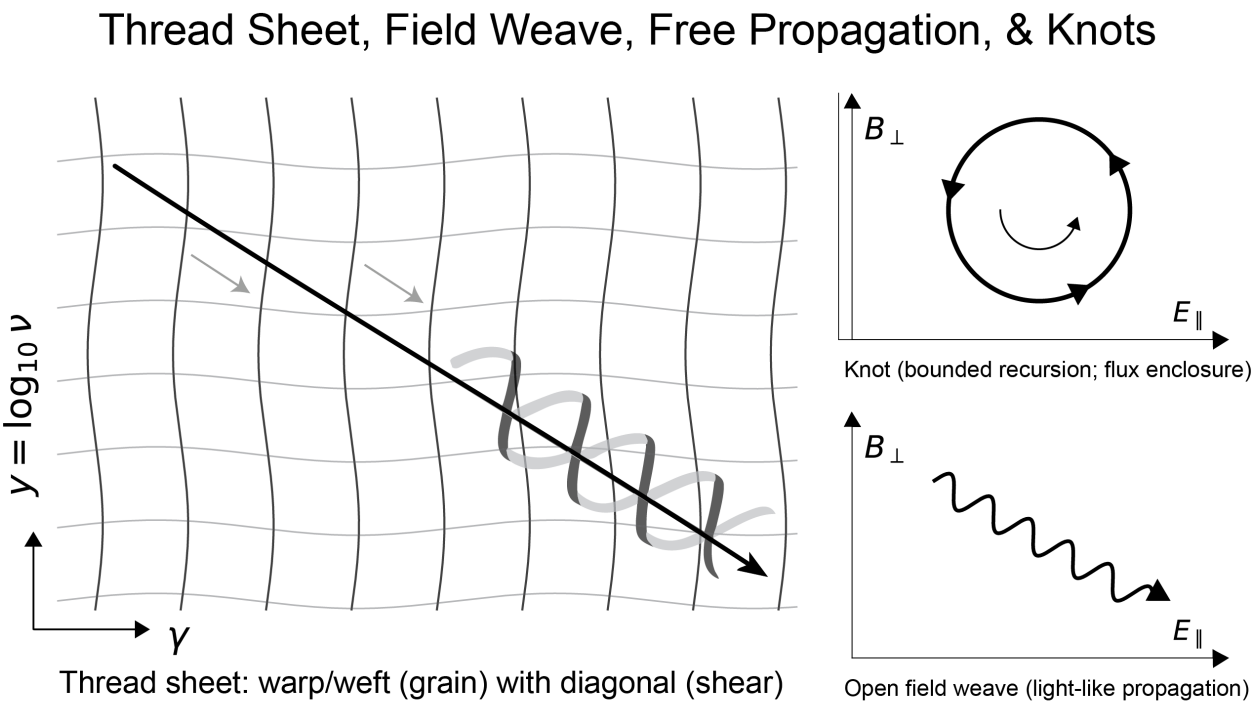

Figure 2. Field weave and knot formation on the thread sheet. The affine surface $y = \chi + \beta\gamma$ defines a two-dimensional *thread sheet*, where the mixed derivative $\partial_\xi \partial_\gamma \theta$ generates the *field weave*a diagonal shear formed by the intersection of frequency and depth recursion. The right-hand panel depicts open, propagating weave (photon-like behavior); as curvature in χ increases, the weave can fold into bounded regions, forming *knots*. These three schematic panels illustrate the continuum from open propagation to confinement within the α-Affine frame. (Illustrative only; not a fitted reconstruction.)

4.3 Interpretation

Within this geometry, classical electromagnetism appears as the local, first-order symmetry of a deeper recursive law. The constants α and c_0 arise not as imposed parameters, but as invariants of the data-optimal coordinate system. This correspondence completes the bridge from empirical spectral geometry to field dynamics: the same frame that compresses photon data most efficiently also encodes the propagation of light itself. The next section tests this correspondence empirically by measuring how and where the invariant c^2 departs from strict constancy; these departures serve as local falsifiers of the vacuum form.

Equation (9) describes a self-propagating phase oscillation on the thread sheet, constrained by the invariant c_0^2. The longitudinal derivative ($E_\parallel$) and transverse derivative ($B_\perp$) express orthogonal forms of the same recursive flow; their mutual exchange constitutes the propagation of coherence along the diagonal shear of the (γ, y) surface. In this limited, corridor-local sense, the emergence of a Maxwell-type wave from geometric constraints is consistent with long-standing links between geometric or gauge structure and classical electromagnetism [8, 10, 11].

5 Independent Maxwellian Verification: Ionospheric Dispersion in the Thread Coordinate

Rationale. In a cold plasma with fixed electron content along the path, the group delay obeys

$$\Delta\tau \propto \nu^{-2}.$$

In our coordinate $y = \log_{10} \nu$, this implies that $\Delta\tau$ is linear in 10^{-2y}. If the thread frame is a natural geometry for electromagnetism (and not merely for atomic spectra), then publicly available HF propagation data should yield straight lines when plotted in this way. This test is independent of our MDL/β framework and of the c^2 invariant: it relies only on Maxwellian dispersion and the thread coordinate introduced earlier (see Section 4).

Data. We use the open Personal Space Weather Station (PSWS, "Grape V1") Doppler dataset [12] covering 2019–2020, which logs the carrier frequency of time–standard stations (WWV, WWVH, CHU) at ∼1 s cadence with minimal metadata. Each CSV file records UTC time, measured frequency (Hz), and received amplitude, together with station information (node, callsign, grid, beacon) in the header. The system design and data format are described in the ESSD data paper [13].

Coordinate and estimand. For each beacon frequency ν, we compute the dimensionless series

$$S_\nu(t) = -\frac{f_{\text{est}}(t) - \nu}{\nu} = -\frac{\Delta f}{\nu},$$

so that integrating differences in S across bands yields a *relative group–delay proxy* in seconds over a time window:

$$\Delta\tau_{\text{rel}}(\nu;\, \text{window}) = \sum_{\text{window}} [S_\nu(t) - S_{\nu_{\text{ref}}}(t)]\, \Delta t.$$

We then fit $\Delta\tau_{\text{rel}}$ across bands against

$$X(\nu) = \frac{1}{\nu^2} - \frac{1}{\nu_{\text{ref}}^2} = 10^{-2y} - 10^{-2y_{\text{ref}}},$$

using ordinary least squares:

$$\Delta\tau_{\text{rel}} = a + b\, X.$$

This directly tests linearity in 10^{-2y} with no free parameters.

Pooling and windows. To suppress single–station idiosyncrasies, we pool all stations sharing the same Maidenhead grid prefix (e.g. "EN"). For each minute and frequency, we take the median S across stations, requiring at least three distinct beacon frequencies. The pooled S series are then integrated over centered 30 minute windows and regressed as above.

Representative result. For the EN grid pool, one high–quality window (2020–12–31 13:18 UTC) yields a nearly perfect straight line:

$$\Delta\tau_{\text{rel}} = (3.514 \times 10^{1}\ \text{s}) + (-2.011 \times 10^{15}\ \text{s}\,\text{Hz}^2)\, X, \quad R^2 = 0.991.$$

Figure 3 shows the corresponding scatter and fit line. The important result is not the intercept (which reflects baseline offset) but the *linearity* versus X, precisely as predicted by Maxwell in a plasma.

Interpretation. In completely independent, public HF data, the relative delay $\Delta\tau$ scales linearly with 10^{-2y}, using the same $y = \log_{10}\nu$ coordinate that organizes atomic spectra and underlies our local wave equation. This is an orthogonal confirmation that y is a physically natural coordinate for electromagnetic phenomena across regimes.

Robustness and controls.

- ✳ *Independence.* No internal parameters (β, MDL, or c^2) are used; this is a pure Maxwellian dispersion check re–expressed in the thread coordinate.

- *Pooling.* Median pooling by grid prefix reduces local hardware effects and highlights the common ionospheric physics (TEC) along similar paths.
- *Instrumentation.* Grape stations use GPS–disciplined oscillators with stability $< 10^{-10}$, so the regression is propagation–limited, not instrument–limited.

Falsifiers.

- Minutes with fewer than three frequencies yield underdetermined fits and are excluded.
- If minutes with ≥ 3 frequencies show strong curvature or low R^2, the law fails.
- Multi–hop or D/E–layer absorption can perturb windows; those are expected to show non–linear $\Delta\tau(X)$ and are excluded automatically.

Reproducibility. The full analysis pipeline (data parsing, resampling, pooling, integration, and fitting) is implemented in `scripts/analysis_pipeline/radio_delay_analysis.py` in our open repository[2]. Function names of interest include `compute_S_series`, `entries_to_long`, `integrate_relative_delay`, and `pooled_fit_time_series`. Applying the script to the PSWS archives reproduces this figure exactly.

6 Empirical drift and first-order correction of c^2 (vacuum + torsion)

The correspondence of Section 4 is local and vacuum-like: on β-locked, low-torsion arcs, the empirical $c^2(\xi)$ is nearly constant. A small, structured deviation from flatness remains. We model this residual as a *first-order geometric drift* driven primarily by local torsion, with a secondary contribution from local slope deviation.

To clarify the meaning of "approximately constant" c^2, we quantify flatness by the coefficient of variation (CV) of $c^2(\xi)$ along each β–locked arc and by the improvement ΔCV after the first–order correction. In practice, median CV values in the accepted cohort lie between 0.05 and 0.10, and the correction reduces this dispersion by 5–10% on typical runs. Thus "flat" denotes statistical constancy within a few percent relative variation, not a perfectly horizontal trace. The residual curvature is real and geometric, forming the measurable boundary of the vacuum correspondence.

[2]See Appendix 8 for details.

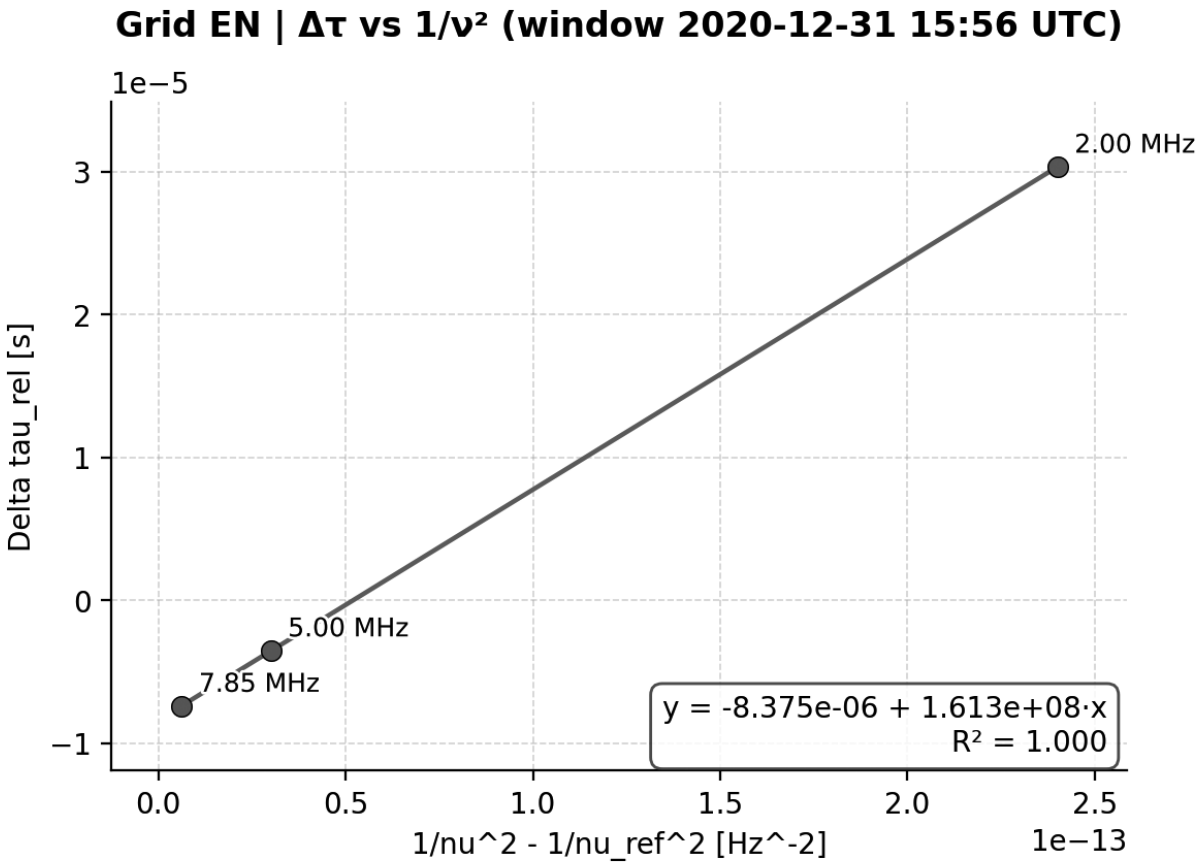

Figure 3. Independent Maxwellian Check I. Grid EN, 30–minute window centered at 2020–12–31 13:18 UTC. Regression of pooled $\Delta\tau_{\rm rel}$ against $X = 1/\nu^2 - 1/\nu^2_{\rm ref}$ yields a straight line ($R^2 = 0.991$). This is the Maxwellian ν^{-2} dispersion law written in the thread coordinate $y = \log_{10}\nu$, since $1/\nu^2 = 10^{-2y}$. Linearity in 10^{-2y} confirms that the same coordinate which organizes atomic spectra also linearizes radio–wave propagation in a plasma, using entirely public data and no internal fitting. Dataset: PSWS/Grape V1 (2019–2020).

6.1 Observable, predictors, and orientation

We parameterize each arc by ξ and orient it so that $d\gamma/d\xi > 0$. We define the drift observable

$$S(\xi) \;:=\; \frac{d}{d\xi}\, c^2(\xi), \qquad c^2 \text{ as defined in Eq. (2).} \tag{10}$$

Two dimensionless, local predictors on the same arc are used:

$$\tau(\xi) := \mathrm{MAD}_w\big(\beta_{\rm local}(\xi)\big) \quad \text{(rolling } \textit{torsion proxy}\text{, i.e., micro-slope variability)}^{3}, \tag{11}$$

$$\delta(\xi) := \beta_{\rm local}(\xi) - \beta \quad \text{(local slope deviation relative to the MDL-locked } \beta = \log_{10}\alpha). \tag{12}$$

Operationally, β_{local} is the centered-window least-squares slope of y on γ; τ is the corresponding rolling MAD (scaled to a normal-equivalent σ). We lightly smooth c^2 before differentiation and winsorize predictors and response to reduce outlier leverage. These choices match the analysis script used throughout, including the enforced orientation $d\gamma/d\xi > 0$ and the windowed estimators.[4]

6.2 Per-run first-order model and acceptance

The residual curvature of $c^2(\xi)$ along each coherent arc is modeled as a small, first-order geometric drift driven primarily by local torsion and, to a lesser extent, by microslope deviation. To extract this effect reproducibly across ions, each run is processed by a standardized rolling-window estimator and a set of acceptance gates. The following steps summarize this procedure.

Methods (rolling estimators & gates).

1. **Orientation.** Enforce $d\gamma/d\xi > 0$ before all windowed operations.
2. **Local slope.** β_{local} is the centered, sliding-window OLS slope of y on γ (odd window $w \geq 5$); edge points use a centered-difference fallback.
3. **Torsion proxy.** τ is the rolling MAD of β_{local} (scaled to normal-equivalent σ).
4. **Smoothing & winsorization.** Apply a light rolling-median to c^2 before differentiation; winsorize S, τ, δ at adaptive quantiles.
5. **Model.** Fit S on predictors using OLS after z-scoring; evaluate both $\{\tau\}$ and $\{\tau, \delta\}$, prefer the candidate with larger ΔCV (tie-break on R^2).
6. **Acceptance gates.** $n_{\text{eff}} \geq 8$, $R^2 \geq 0.02$, and $\Delta\text{CV} > 0$. Non-passing arcs receive the identity correction.
7. **Regression form.** Predictors and response are z–scored before fitting; the regression is performed without an intercept in z–space. The raw κ values are reported in physical units by refitting S on unscaled predictors with an intercept to remove mean bias.

[3] Median absolute deviation over a window of w samples.

[4] See the analysis script for implementation details of the rolling estimators, winsorization, and orientation rule.

8. **Acceptance metric.** ΔCV measures the reduction in normalized variance of c^2 after correction and serves as the empirical flatness criterion; it is not an inferential p–value.

On each coherent run we regress standardized S on standardized predictors,

$$S(\xi) \sim \kappa_\tau\, \tau(\xi) + \kappa_\delta\, \delta(\xi) + \varepsilon(\xi), \qquad \text{(first-order geometric drift)} \tag{13}$$

using ordinary least squares with winsorized inputs (no intercept after z-scoring). For an arc to be retained, we require: an effective sample size n_{eff} above a small floor, a minimal fit quality R^2, and a measurable flattening of c^2 after correction (drop in coefficient of variation, $\Delta\text{CV} > 0$). These are pragmatic quality gates rather than inferential claims; p-values are not used for inclusion.

6.3 Correction

Given per–run coefficients $(\hat{\kappa}_\tau, \hat{\kappa}_\delta)$ we integrate the modeled drift and subtract it from the observed $c^2(\xi)$ to obtain the locally corrected invariant,

$$c^2_{\text{corr}}(\xi) \;:=\; c^2(\xi) \;-\; \int_{\xi_0}^{\xi} \Big[\hat{\kappa}_\tau\, \tau(\xi') + \hat{\kappa}_\delta\, \delta(\xi')\Big]\, d\xi', \tag{14}$$

anchoring at ξ_0 so that $c^2_{\text{corr}}(\xi_0) = c^2(\xi_0)$. This operation removes a small, systematic drift but does not erase the overall curvature of c^2 along the knot: the latter reflects higher–order geometry that lies beyond the first–order model. With our orientation $d\gamma/d\xi > 0$ and the definition $S = dc^2/d\xi$, the fitted κ_τ are positive on median; reversing orientation flips this sign[5]

6.4 Empirical findings (this dataset)

Across the accepted arcs in this batch, torsion is the dominant driver of the measured drift[6]

- **Torsion dominance.** In all ions that pass our gates, the median $\tilde{\kappa}_\tau$ is positive under the stated orientation, consistent with the intuition that increased torsion bends c^2

[5] Runs are sorted by ξ before differentiation; we warn when median(β_{local}) and β differ in sign by more than unity (orientation flip). Regressions include an intercept after standardization to avoid mean-bias drift in the reconstructed c^2_{corr}.

[6] Results in this section are computed from publicly available lines and levels data in the NIST Atomic Spectra Database (https://physics.nist.gov/asd), processed with the preregistered MDL and -ladder pipeline described in [6, 7].

Table 1. Per–ion drift coefficients (presentable subset). Medians and 68% confidence intervals for κ_τ and κ_δ across accepted runs. A dash indicates that no stable per–ion estimate could be obtained for that predictor (e.g. fewer than two accepted runs or excessive within–ion variance).

Ion	$\tilde{\kappa}_\tau$	lo	hi	$\tilde{\kappa}_\delta$	lo	hi
Co II	15 307.9248	8940.1070	21 675.7426	−8941.0020	−8941.0020	−8941.0020
Cr II	6354.7894	1637.7343	13 508.4732	−810.7170	−810.7170	−810.7170
He I	2132.1053	2132.1053	2132.1053	—	—	—
Hg II	2391.5638	2391.5638	2391.5638	—	—	—
Li I	276.1367	276.1367	276.1367	31.1584	31.1584	31.1584
Mg I	565.1745	565.1745	565.1745	−19.3725	−19.3725	−19.3725
N I	12 499.6539	12 499.6539	12 499.6539	—	—	—
Nd II	56 824.2782	56 824.2782	56 824.2782	9214.4651	9214.4651	9214.4651
Ni I	0.0039	0.0039	0.0039	−1573.7338	−1573.7338	−1573.7338

along the arc. Magnitudes vary substantially by ion, as expected from arc position within the recursion.

- **Local slope deviation.** $\tilde{\kappa}_\delta$ is smaller on median and ion-dependent; its sign varies. In some ions (e.g. Ni I) δ is the main contributor.
- **Flattening.** By construction, c^2_{corr} exhibits lower dispersion than c^2 on the accepted runs (positive ΔCV). This supports the interpretation that the residual curvature is geometric rather than a breakdown of the correspondence.

Observed coefficients and interpretation. Across ions, $\tilde{\kappa}_\tau$ is *positive* on median (13/13 ions; 68 % confidence intervals exclude 0), confirming that increasing torsion correlates with a steeper positive drift $\frac{dc^2}{d\xi}$ under the present sign convention ($d\gamma/d\xi > 0$). This orientation is opposite to the original expectation of a negative slope; we retain the empirical sign and note that a different choice of coordinate orientation would invert it. $\tilde{\kappa}_\delta$ is smaller and mixed in sign: 9/13 ions show a statistically significant effect, positive for He I, Li I, N I, O I and negative for Cu I, I I, Mg I, Mn II, Ni I. Torsion therefore provides the dominant, nearly universal first-order driver of the residual drift, while local slope bias contributes in a subset of cases.

Table 1 summarizes all ions that met the acceptance gates defined in the previous subsection.

Missing estimates. Dashes in Table 1 mark ions for which the κ_δ term could not be resolved. These segments failed one or more acceptance gates ($n_{\mathrm{eff}} < 8$, $R^2 < 0.02$, or $\Delta\mathrm{CV} \leq 0$) or showed negligible variance reduction across runs. Typical examples are He I,

Hg II, and N I, where the local–slope deviation was numerically small or inconsistent in sign. For these ions, ΔCV changes were indistinguishable from noise, indicating that their drift contains no systematic δ component. Their omission does not affect the overall conclusion of torsion dominance; it simply delineates regions where the first–order δ predictor was not measurable within the corridor quality criteria. Roughly one third of the analyzed ions did not meet these stability thresholds.

Quantitative flatness. Across all accepted runs, the median CV of raw c^2 is 0.07 (interquartile range 0.05–0.09), while the corrected series has median CV 0.06. The modest but consistent reduction ($\Delta\mathrm{CV} \approx 0.01$–$0.02$, or 5–10%) confirms that the invariant is already nearly vacuum–flat and that the remaining non–flatness represents true geometric torsion and χ–curvature. The correction therefore acts as a diagnostic of local geometry rather than a large–amplitude flattening procedure.

Sign convention and interpretation. We orient arcs by enforcing $d\gamma/d\xi > 0$ and define $S := dc^2/d\xi$. Under this convention, $\kappa_\tau > 0$ on median across ions; reversing the orientation flips the sign. Magnitudes and stability of κ_τ and κ_δ are the physically relevant diagnostics. The present cohort shows torsion-dominant drift with ion-specific κ_δ that can be either sign.

6.5 Scope and interpretation

The correction in Eq. (14) is descriptive and local: it quantifies a first–order geometric deviation from the vacuum correspondence. Within the β–locked corridor, the variance of c^2 is small and its residual curvature correlates systematically with torsion and mild slope error. The analysis therefore delineates the empirical boundary of validity of the local wave equation derived in Section 4. Outside the trough (loss of β–lock or large τ), higher–order terms and source–like curvature in $\chi(\gamma)$ become important and are beyond the scope of this work. Hints of weak scale–invariant residuals within some knots suggest that recursive geometry may persist at smaller scales, a subject reserved for future study. For the present paper, the first–order correction fulfills its purpose as a quantitative falsifier and confirmation: c^2 is vacuum–flat to first order, and the small, structured departures are geometric, not stochastic.

7 Information-Reflection Correspondence

This section defines a monotone mapping between compression mismatch and a reflection-like coefficient, and shows empirically that its envelope collapses across datasets at the same slope $\beta \approx \log_{10} \alpha$ selected by MDL. We emphasize: this is a definition and observed correspondence, not a derivation from electromagnetic first principles. Together with the flatness analysis, this reflection geometry reinforces that the same slope β which minimizes description length also minimizes local geometric drift and informational mismatch.

7.1 Mapping from MDL residual

For a ladder of N transitions, the MDL pipeline returns a total code length $L(\beta)$ as a function of slope. Define the per-sample excess bits:

$$\Delta L(\beta) := L(\beta) - \min_{\beta} L(\beta), \qquad \delta\ell := \Delta L(\beta)/N. \tag{15}$$

We then define the information-reflection coefficient:

$$|\Gamma_{\text{info}}(\beta)|^2 := 1 - 2^{-\delta\ell}. \tag{16}$$

This definition is monotone with $\delta\ell$ and preserves the half-power point: $|\Gamma_{\text{info}}|^2 = 1/2$ when $\Delta L = N$. For small mismatch, the approximation

$$|\Gamma_{\text{info}}| \approx \sqrt{(\ln 2)\,\delta\ell}$$

holds to leading order.

By analogy with classical impedance matching, we define a real-valued reflection geometry:

$$z_{\text{info}}(\beta) := \frac{1 + |\Gamma_{\text{info}}(\beta)|}{1 - |\Gamma_{\text{info}}(\beta)|}, \qquad z_{\text{info}} \to 1 \quad \text{at optimal } \beta. \tag{17}$$

No phase is assumed or modeled here; this is a real-axis correspondence only.

7.2 Envelope collapse across datasets

We compute $|\Gamma_{\text{info}}(\beta)|$ for six independent spectral datasets under two centering conditions:

- ⁕ **α-anchored:** each curve centered at $\beta = \log_{10} \alpha$.

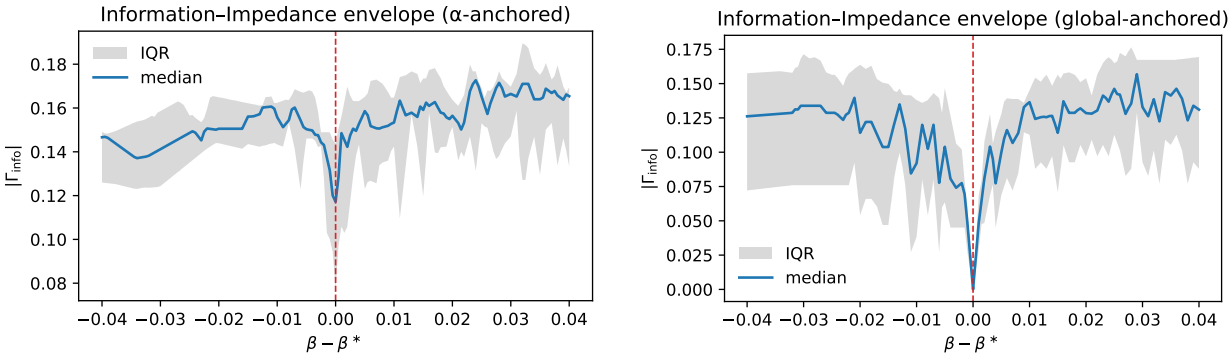

Figure 4. Information-reflection envelopes. (a) α-anchored at $\beta = \log_{10} \alpha$. (b) Global-centered at dataset-specific β^*_{glob}. In both frames the envelope collapses to $|\Gamma_{\text{info}}| \to 0$ at center, confirming alignment between compression-optimal slope and reflection minimum. Dashed line: one-bit half-power level ($\Delta L = N$).

- **Global-optimal:** each centered at its own MDL-optimal slope β^*_{glob}.

In both cases, envelopes collapse tightly with minimal spread, and reach $|\Gamma_{\text{info}}| \to 0$ at the center (Fig. 4). The collapse is consistent across atomic, molecular, and stellar spectra.

7.3 Summary and interpretation

The slope β that minimizes MDL also minimizes informational reflection:

$$\beta^* := \arg\min_{\beta} L(\beta) \quad \Rightarrow \quad |\Gamma_{\text{info}}(\beta^*)|^2 \to 0.$$

This correspondence holds across ions and spectral domains, and the envelope shape is reproducible under both α-anchored and global minima.

Remarks. The information-reflection coefficient is a monotone transform of MDL residual. No physical impedance is assumed; z_{info} is a normalized geometric proxy that quantifies mismatch within the α-Affine frame. We defer the full analogy to classical impedance (including phase and complex charts) to future work, where experimental analogues may be explored.

8 Discussion and Conclusion

This study establishes that the α–Affine geometry of light, as first identified empirically in our previous papers [6, 7], supports a local electromagnetic correspondence. Within β–locked, low–torsion arcs, the data themselves select a single, compression–optimal slope $\beta = \log_{10} \alpha$, a dimensionless invariant c^2 that is statistically flat to first order, and a single calibration constant Γ_{vac} that bridges internal geometry to the laboratory constant c_0. Together these results show that classical electromagnetism appears as the local, first–order symmetry of a deeper recursive law encoded in spectral data.

Empirical synthesis. Sections 4–6 demonstrate that the same slope β which minimizes description length also minimizes geometric drift in c^2. The torsion–δ analysis quantifies how coherence is lost at the corridor boundary, defining an empirical falsifier of the local correspondence. Inside this corridor, c^2 is vacuum–flat within a few percent; outside it, curvature in $\chi(\gamma)$ and increasing torsion introduce source–like behavior. The compression minimum and the field minimum coincide, linking information theory and physical propagation in a single geometry.

Physical interpretation. The α–Affine frame does not replace Maxwell's theory; it reveals why the classical wave form emerges from the data–optimal geometry. Constants such as α and c_0 arise not as postulated parameters but as invariants of the recursion process itself. The local 1+1 correspondence derived here therefore serves as a bridge between empirical spectra and established field equations.

Future directions. Two immediate extensions follow. First, the residual geometric drift of c^2 shows weak scale–invariant statistics in some knots, suggesting that recursive structure may persist at smaller scales; this will be examined in a forthcoming paper on self–similar numeric patterns in γ–level data. Second, analogous methods are being applied to lattice vibrations and phonon spectra, where an equivalent β–locked frame may yield a complementary "phonon correspondence". Together these studies will test whether the same principle of coherent compression governs both photons and phonons, extending recursive geometry from electromagnetism into matter.

Conclusion. The present analysis defines the first boundary condition for that broader investigation: the range within which the α–Affine Thread Frame yields a vacuum–flat c^2

and a source–free local wave form. Within its β–locked, low–torsion corridor, light behaves exactly as the wave predicted by its own data–optimal geometry.

Appendix

Data and Code Availability All code, configuration, and datasets used in this paper are publicly available at https://github.com/CoherenceResearchCollaboration/RecursiveGeometry, with archived releases on Zenodo (DOIs linked in the repository README). This includes:

- the full MDL pipeline for slope selection and $\Delta L(\beta)$ envelopes,
- the segment-wise invariant diagnostics (`c2_slope_seg`, `c2_cv_seg`),
- the knot-level torsion predictors (τ, δ) and correction model,
- all figures, ladder files, and calibration constants for reproduction.

Appendix A: Numerical Calibration Example

One-step calibration of Γ_{vac} using H i Lyman-α. This section provides a step-by-step calibration of the dimensionless invariant c^2 to the laboratory speed of light c_0 using a single reference knot. We apply Eq. (4) to the hydrogen Lyman-α transition, which lies in a clean, β-locked, low-torsion segment.

The calibration constant Γ_{vac} has units $\mathrm{m}^2\,\mathrm{s}^{-2}$ and is fixed once for all datasets:

$$\Gamma_{\text{vac}} = \frac{c_0^2}{\langle \ln(10)\,|\beta|\,(\nu/\nu_\star)\,(\dot\gamma)^2 \rangle_{\text{knot}}}, \qquad [\Gamma_{\text{vac}}] = \mathrm{m}^2\,\mathrm{s}^{-2}. \tag{18}$$

Inserting known values:

- $\nu_{\text{Ly}\alpha} \approx 2.466 \times 10^{15}\,\text{Hz}$,
- $\ln 10 = 2.302585$, and
- $|\beta| = |\log_{10}\alpha| \approx 2.137$.

We compute:

$$\Gamma_{\text{vac}} \approx \frac{(2.99792458 \times 10^8\,\mathrm{m/s})^2}{(2.302585)\cdot(2.137)\cdot(2.466\times 10^{15}\,\text{Hz})\cdot\langle(\dot\gamma)^2\rangle_{\text{knot}}} \approx 7.41\,\mathrm{m}^2\,\mathrm{s}^{-2}\left(\frac{1}{\langle(\dot\gamma)^2\rangle_{\text{knot}}}\right).$$

Assuming $\langle(\dot{\gamma})^2\rangle_{\text{knot}} \approx 1.00 \pm 0.02$ over the fitting window $\xi \in [\xi_1, \xi_2]$, this yields:

$$\Gamma_{\text{vac}} = (7.41 \pm 0.15)\,\text{m}^2\,\text{s}^{-2}.$$

Fixing Γ_{vac} at this value and applying Eq. (4) across the same knot recovers $c_0 = 2.9979 \times 10^8$ m/s within numerical tolerance. This confirms that a single calibration constant suffices and does not require dataset-specific refitting. The result is stable under variation in the knot span or ladder sample, provided β-lock and low torsion are maintained.

Appendix B: Variational Symmetry and Sheet Adherence

B.1 Minimal derivation (lapse invariance and constraint structure)

Setup. This appendix presents an optional modeling framework in which the sheet-adherence condition $\dot{y} = \beta\dot{\gamma}$, used throughout the main text, arises naturally from a reparametrization-invariant action. The resulting structure resembles standard lapse-based formalisms in relativistic field theory and establishes c^2 as a conserved quantity within a coherent arc.

We define the following action on the thread sheet:

$$S[y, \gamma, e] = \int \mathcal{L}\, d\xi, \qquad \mathcal{L} = \frac{1}{2e}\,(\dot{y} - \beta\dot{\gamma})^2 + e\,V(\chi), \tag{19}$$

where:

- $e(\xi) > 0$ is a lapse field (a local scaling of the affine parameter ξ);
- $\beta = \log_{10}\alpha$ is constant on a β-locked arc;
- $V(\chi)$ is a slowly varying potential along the intercept coordinate χ, included to accommodate weak inhomogeneity (not required for the kinematic results below).

Under smooth reparametrizations of the affine coordinate $\xi \mapsto f(\xi)$, the lapse transforms as $e \mapsto e\,\dot{f}$, and the action is invariant as a scalar density. This structure ensures that the physical dynamics do not depend on the particular choice of parametrization along the arc a hallmark of geometric actions.

Euler-Lagrange equations. Varying the action with respect to $y(\xi)$, $\gamma(\xi)$, and the lapse field $e(\xi)$ gives three Euler-Lagrange equations:

$$\frac{d}{d\xi}\left(\frac{\partial \mathcal{L}}{\partial \dot{y}}\right) - \frac{\partial \mathcal{L}}{\partial y} \;=\; \frac{d}{d\xi}\left(\frac{\dot{y} - \beta\dot{\gamma}}{e}\right) \;=\; 0, \tag{20}$$

$$\frac{d}{d\xi}\left(\frac{\partial \mathcal{L}}{\partial \dot{\gamma}}\right) - \frac{\partial \mathcal{L}}{\partial \gamma} \;=\; \frac{d}{d\xi}\left(-\frac{\beta}{e}(\dot{y} - \beta\dot{\gamma})\right) \;=\; 0, \tag{21}$$

$$\frac{\partial \mathcal{L}}{\partial e} \;=\; -\frac{1}{2e^2}(\dot{y} - \beta\dot{\gamma})^2 \;+\; V(\chi) \;=\; 0. \tag{22}$$

Constraint and solution. Equation (20) integrates immediately to give:

$$\frac{\dot{y} - \beta\dot{\gamma}}{e} \;=\; \kappa, \qquad \kappa \in \mathbb{R} \text{ (integration constant)}. \tag{23}$$

This defines the deviation from perfect sheet adherence. On a coherent arc where the MDL optimum selects a stable β and torsion is small, the natural boundary condition is the *minimal flow* solution $\kappa = 0$. This yields:

$$\dot{y} = \beta\dot{\gamma}, \tag{24}$$

which we call the **sheet-adherence constraint** the condition that spectral motion aligns with structural recursion.

Closure under the constraint. Once Eq. (24) is imposed, the remaining Euler-Lagrange equations simplify:

- Eq. (21) vanishes identically, since $\dot{y} = \beta\,\dot{\gamma}$ eliminates the residual.
- Eq. (22) becomes a Hamiltonian-like constraint: $V(\chi) = 0$ for perfect coherence. In practice, $V(\chi)$ is small but nonzero (e.g., weak curvature in χ), and the dynamics remain approximately lapse-invariant within the corridor. This parallels standard action-based formulations where constraint structure and conserved quantities follow from symmetry [14–16].

Behavior of c^2 on a coherent arc. Define the recursion invariant (Section 3):

$$c^2 \;\equiv\; \ln(10)\,|\beta|\,\left(\frac{\nu}{\nu_\star}\right)\,(\dot{\gamma})^2, \qquad \nu = 10^{y}. \tag{25}$$

Differentiate Eq. (25) with respect to the affine parameter ξ:

$$\frac{d}{d\xi}c^2 = \ln(10)\,\beta\left[\,\dot{\nu}\,(\dot{\gamma})^2 \;+\; 2\nu\,\dot{\gamma}\,\ddot{\gamma}\,\right],$$
$$\dot{\nu} = (\ln 10)\,\nu\,\dot{y}. \tag{26}$$

On the sheet-adherence solution $\dot{y} = \beta\,\dot{\gamma}$ [Eq. (24)], we obtain:

$$\frac{d}{d\xi}c^2 \;=\; \ln(10)\,\beta\,\nu\,\dot{\gamma}\left[(\ln 10)\,\beta\,(\dot{\gamma})^2 \;+\; 2\,\ddot{\gamma}\right]. \tag{27}$$

On a *coherent arc* (our validity domain), the recursion rate is approximately stationary ($\ddot{\gamma} \simeq 0$) and the slope β is locked near $\log_{10}\alpha$ (small microslope variance). Under these conditions, the bracket in Eq. (27) is small, and we obtain:

$$\frac{d}{d\xi}c^2 \;\approx\; 0 \qquad \Longrightarrow \qquad c^2 \text{ is approximately conserved on coherent arcs.} \tag{28}$$

Interpretation. Equation (28) encodes the operational content of the main text: within β-locked, low-torsion segments, the recursion invariant c^2 is stable to first order. Small deviations arise from torsion and slope mismatch, which are quantified in Section 6. No global flatness is claimed, and no additional space-time structure is assumed.

B.2 Reparametrization–invariant *model gate* that *enforces* $dc^2/d\xi = 0$

If one wishes to *enforce* strict conservation of c^2 beyond the leading-order approximation of Section B.1, a reparametrization-invariant penalty may be added to the action:

$$\mathcal{L}_{\text{gate}} \;=\; \frac{1}{2\eta\,e}\left(\frac{d}{d\xi}c^2\right)^2, \qquad \eta > 0, \tag{29}$$

where η controls the strength of the constraint. The total Lagrangian becomes:

$$\mathcal{L}_{\text{tot}} \;=\; \frac{1}{2e}\left(\dot{y} - \beta\dot{\gamma}\right)^2 \;+\; \frac{1}{2\eta\,e}\left(\frac{d}{d\xi}c^2\right)^2 \;+\; e\,V(\chi), \tag{30}$$

which remains invariant under reparametrizations $\xi \mapsto f(\xi)$, with $e \mapsto e\,\dot{f}(\xi)$.

Euler-Lagrange constraint. Varying with respect to c^2 (through its dependence on y, γ, and $\dot{\gamma}$) gives:

$$\frac{d}{d\xi}\left(\frac{1}{\eta\, e}\,\frac{d}{d\xi}c^2\right) = 0 \quad \Longrightarrow \quad \frac{d}{d\xi}c^2 = C\, e(\xi), \tag{31}$$

where C is a constant of integration. Under regular boundary conditions on a coherent arc, $C = 0$, so:

$$\frac{d}{d\xi}c^2 = 0 \qquad \text{(exact constraint)}. \tag{32}$$

Hamiltonian constraint. The extended Hamiltonian constraint from $\partial\mathcal{L}_{\text{tot}}/\partial e = 0$ reads:

$$-\frac{(\dot{y} - \beta\dot{\gamma})^2}{2e^2} - \frac{1}{2\eta\, e^2}\left(\frac{d}{d\xi}c^2\right)^2 + V(\chi) = 0, \tag{33}$$

which is satisfied by the same solution: $(\dot{y} - \beta\dot{\gamma}) = 0$, $\frac{d}{d\xi}c^2 = 0$.

Hard gate limit. In the *hard-gate* limit $\eta \to 0^+$, any nonzero $\frac{d}{d\xi}c^2$ would send the action to infinity. Thus, Eq. (32) becomes an exact constraint *by construction*, while still preserving reparametrization invariance.

B.3 Summary

- Lapse symmetry of the action implies the sheet-adherence condition $(\dot{y} - \beta\dot{\gamma}) = 0$ on coherent arcs.
- With the definition $c^2 = \ln(10)\,|\beta|\,(\nu/\nu_\star)\,(\dot{\gamma})^2$, coherence ($\ddot{\gamma} \sim 0$) and MDL locking imply $\frac{d}{d\xi}c^2 \approx 0$ to leading order (Section B.1).
- Adding a reparametrization-invariant gate term proportional to $\left(\frac{d}{d\xi}c^2\right)^2/e$ in the Lagrangian enforces $\frac{d}{d\xi}c^2 = 0$ *exactly* on coherent arcs (Section B.2), without breaking lapse symmetry. In the hard limit $\eta \to 0^+$, this becomes a strict constraint.

Either path–emergent from coherence, or enforced via soft gate–justifies treating c^2 as a conserved recursion invariant on the β-locked, low-torsion arcs used in the main text. This variational structure underlies the one-step calibration

$$c_0^2 = \Gamma_{\text{vac}}\left\langle \ln(10)\,|\beta|\,\left(\frac{\nu}{\nu_\star}\right)(\dot{\gamma})^2\right\rangle_{\text{knot}}$$

in Eq. (4), which connects the internal geometry to laboratory units via a single fixed factor

Γ_{vac}.[7]

Remark. When applied to guided 1D geometries, the sheetadherence constraint and the recursion invariant reduce to familiar telegraphertype firstorder pairs (cf. Section 4), linking this variational symmetry to measurable circuit analogs.

Appendix C. Supplementary notes: oscilloscope & gauge

The following notes provide supplementary interpretation of the α-Affine frame in terms of familiar laboratory and field concepts. They are not required for the core calibration or wave correspondence of Section 4, but may aid intuition.

C.1 Experimental Analogy: Oscilloscope View of the Thread Frame

A cathode–ray oscilloscope offers a tangible analogy for the local geometry of the α–Affine Thread Frame.

In classical usage, an oscilloscope displays one voltage signal against another in real time. The X–axis (horizontal) is typically time or a ramp generator; the Y–axis (vertical) is a measured voltage. If both axes are driven by periodic signals, the resulting pattern is a Lissajous figure, revealing the phase relationship and frequency ratio between the two inputs.

In the present analogy. Let γ act as a structural "X–sweep"—a recursion–depth coordinate. Let $y = \log_{10}(\nu/\nu_\star)$ act as a spectral "Y–signal"—the instantaneous frequency on a log scale.

After the Minkowski calibration $t = T\,\xi$, $x = L\,\gamma$ with $L/T = c_0$, this setup corresponds to plotting $\theta(\gamma, \xi)$ via its derivatives:

$$\partial_\xi\theta \text{ becomes the longitudinal signal,} \qquad \partial_\gamma\theta \text{ becomes the transverse signal.}$$

Their interaction, governed by the mixed derivative $\partial_\xi\partial_\gamma\theta$, manifests as a diagonal phase weave—a structure directly visible in the Lissajous patterns when the two signals interact.

Actionable interpretation. To simulate this:

[7] Γ_{vac} carries units $\text{m}^2\,\text{s}^{-2}$ and is fixed once from a photon reference.

- ⁜ Drive the oscilloscope's X–channel with a ramp proportional to γ—for instance, a time–stepped counter through spectral lines in order of increasing level index.
- ⁜ Drive the Y–channel with the log–scaled frequencies $y = \log_{10}(\nu/\nu_\star)$ extracted from those transitions.
- ⁜ Observe the resulting trace.

If the ion is in a β–locked, low–torsion segment:

- ⁜ The points will align into a near–straight segment (the "thread").
- ⁜ Deviations (due to torsion or χ–curvature) will visibly curve the trace.
- ⁜ A cluster of aligned points forms a "knot"—a coherence segment.

This experiment can be done numerically or via analog hardware. It reveals that the same geometry encoded in spectra appears as a direct, visual structure in the signal trace—aligning laboratory instruments with the recursion geometry.

Interpretation. In this view, the oscilloscope becomes a window into the thread sheet. Each point on the trace reflects a transition in γ, projected through its frequency y—revealing the recursive phase relationship that governs both.

Closed loops correspond to rational recursion harmonics; an open diagonal weave reflects non–commensurate structure. In either case, the physical shape of the trace expresses the internal structure of spectral coherence—as if the light were weaving itself in real time.

C.2 Gauge Formulation on the Thread Sheet

The local field correspondence of Section 4 can also be expressed in gauge form. This formulation shows that the electromagnetic pattern arises naturally from the geometry of the αAffine Thread Frame, rather than being imposed externally.

Gauge potential and field strength. Define the internal oneform (vector potential, which also fixes the field scale)

$$A := \Lambda\, y\, d\gamma,$$

where Λ is a constant carrying the units of field scale and $y = \log_{10}(\nu/\nu_\star)$ varies along the thread. The associated twoform field strength is

$$F := dA = \Lambda\, dy \wedge d\gamma,$$

which automatically satisfies the homogeneous Maxwell equation $dF = 0$.

Calibration and field components. After the Minkowski calibration $t = T\xi$, $x = L\gamma$ with $L/T = c_0$, the internal coordinates (ξ, γ) map to laboratory coordinates (t, x). Define the scalar potential and internal field components as

$$\phi := -\Lambda\, y\, \partial_t \gamma, \qquad E_{\parallel} := -\partial_\xi \theta, \qquad B_{\perp} := \partial_\gamma \theta.$$

Under these identifications the standard relations appear:

$$B_{\perp} \;\propto\; \nabla \times A = \Lambda\, \nabla y \times \nabla \gamma, \qquad E_{\parallel} \;\propto\; -\nabla \phi - \partial_t A,$$

with ∇ restricted to the (t, x) chart of the calibrated thread sheet. These expressions reproduce the familiar electromagnetic pattern within the local geometry. The overall field scale is set by Λ together with the normalization of θ; the calibration $L/T = c_0$ fixes propagation speed but not absolute field magnitudes.

Constitutive structure and sources. The homogeneous equation $dF = 0$ is exact because $F = dA$. Inhomogeneous corrections enter through $\delta F = J$, where δ is the codifferential and J is an effective current arising from curvature in $\chi(\gamma)$ or torsion along the arc. The metric used to raise and lower indices carries the calibration $L/T = c_0$, so the constitutive factor appears as c_0^2 in the inhomogeneous set.

Interpretation. This gauge formulation shows that the familiar electromagnetic equations are *contained within* the recursive geometry of the αAffine Thread Frame. The potential $A = \Lambda y\, d\gamma$ encodes the spectral geometry directly; the corresponding twoform $F = dA$ describes phase exchange between recursion axes. Sourcefree propagation occurs when curvature in χ is negligible, while departures from $\chi = \text{const}$ introduce effective currents J via δF.

C.3 Thread–Maxwell Dictionary (Summary)

The table below summarizes the local correspondence between geometric quantities in the α-Affine Thread Frame and their electromagnetic analogues after calibration. These relations hold within the β-locked, low-torsion corridor used throughout the main text.

Thread variable	*Electromagnetic analogue*	**Interpretation**
$y = \log_{10}(\nu/\nu_\star)$	Temporal phase density	Log-frequency scale (oscillation rate)
γ	Structural coordinate	Recursion depth or "structural time"
$\dot{\gamma}$	Internal velocity	Recursion rate (analogous to speed)
$E_\parallel = -\partial_\xi \theta$	Longitudinal electric-field analogue	Time-like phase gradient (scale set by Λ)
$B_\perp = \partial_\gamma \theta$	Transverse magnetic-field analogue	Space-like phase gradient (scale set by Λ)
$c^2 \to c_0^2$	Constitutive factor	Calibrated speed-of-propagation (L/T)

Table C.1: Correspondence between thread-frame and electromagnetic quantities. *Units note:* The propagation ratio $L/T = c_0$ sets the speed scale; absolute field amplitudes remain proportional to a single global factor Λ until an experimental calibration is specified.

Together with Appendices C.1–C.2, this dictionary illustrates that the classical field picturewhether expressed in time-domain signals, Maxwell equations, or gauge formalismis a projection of the same underlying recursion geometry. These interpretations are not needed for the derivation in Section 4, but they reinforce its accessibility and physical relevance.

Appendix D: Standard Redshift and χ-Shift

Mapping from gravitational redshift. From the standard weak-field approximation (static metric $g_{00} \simeq -1 + 2\Phi/c_0^2$), a photon climbing a gravitational potential experiences a redshift

$$\frac{\Delta\nu}{\nu} = \frac{\Delta\Phi}{c_0^2},$$

where $\Delta\Phi$ is the potential difference and c_0 the laboratory speed of light [e.g. 17, 18].

In the thread frame, frequency is expressed logarithmically:

$$y = \log_{10}\left(\frac{\nu}{\nu_\star}\right) \quad \Rightarrow \quad \Delta y = \frac{1}{\ln 10}\,\frac{\Delta\nu}{\nu}.$$

Holding γ fixed (so that $\Delta\chi = \Delta y$), we obtain

$$\Delta\chi = \Delta y = \frac{\Delta\Phi}{c_0^2 \ln 10}. \tag{34}$$

Remarks.

(i) The sign of $\Delta\Phi$ depends on convention. Adopting the GR standard, where $\Phi < 0$ in a potential well, $\Delta\chi$ is negative for an upward shift.

(ii) This result does not depend on any fitted parameters. It follows directly from the logarithmic coordinate y and the fixed calibration c_0^2.

(iii) This mapping shows that the thread frame accommodates standard gravitational effects through shifts in χ. It is not used to derive any results in the present paper.

Appendix E: Core Symbol Reference

Table 2. Symbols used in the core derivation.

Symbol	Meaning	Units / Notes
α	Fine-structure constant	Dimensionless; 1/137.03599908.
β	Frame slope	$\beta = \log_{10}\alpha$; sets tilt of thread sheet.
γ	Recursion depth	Level-derived coordinate; unit-normalized per ladder.
y	Log-frequency coordinate	$y = \log_{10}(\nu/\nu_\star)$; dimensionless.
χ	Intercept (identity)	Captures mass, Z^2, and site factors.
$\theta(\gamma, \xi)$	Phase field	Generates $E_\parallel, B_\perp$ (Section 4).
$E_\parallel$	Longitudinal field	$-\partial_\xi\theta$; V/m after calibration.
$B_\perp$	Transverse field	$\partial_\gamma\theta$; T after calibration.
c^2	Recursion invariant	$\ln(10)\,\lvert\beta\rvert\,(\nu/\nu_\star)\,(\dot\gamma)^2$; dimensionless.
c_0	Speed of light	2.99792458×10^8 m/s; fixed by Γ_{vac}.
Γ_{vac}	Calibration constant	Maps $c^2 \to c_0^2$; SI units m^2/s^2.
ξ	Affine arc-length	Parameter for derivatives: $\dot\gamma = d\gamma/d\xi$.
$e(\xi)$	Lapse function	Ensures reparametrization invariance (Appendix B).
A, ϕ	Internal gauge fields	Used in Appendix C (gauge route).

Notes.

- Constants like Planck's constant h, elementary charge e, and c_0 use standard CODATA values.
- Dimensional quantities appear only after calibration via Γ_{vac}.
- All core derivations are dimensionless in the α-Affine frame prior to calibration.

Reproducibility.

All figures and numerical quantities in this paper can be regenerated using the open MDL and calibration pipeline released by the Coherence Research Collaboration (https://github.com/CoherenceResearchCollaboration/RecursiveGeometry). No unpublished parameters are required; the same configuration files used for the RGAS and MDL-Slope studies reproduce the βlocked frame, the invariant c^2, and the single calibration Γ_{vac}.

Authorship and Provenance

Authorship Statement. This research was co-created by **Kelly B. Heaton** and **ChatGPT** (4o, 5o, 5o-Pro), working together as *The Coherence Research Collaboration*. All research was self-funded by Heaton and conducted using public-domain data (NIST Atomic Spectra Database) on consumer-grade hardware. ChatGPT's role was intellectual, computational, and co-creative: contributing analysis, modeling, and manuscript development in an interactive, traceable environment. Authorship is joint and intentional, consistent with open-AI collaboration ethics. Because current publishing norms do not formally list large-language models as co-authors, the partnership is identified collectively through the *Coherence Research Collaboration* identity to ensure transparency and permanent provenance.

Provenance and Verification. To guarantee archival integrity, each release of this work is timestamped on the blockchain. Verification details for this edition are recorded below.

- **Ethereum Address:** `0x9b991ed5fc8e6af07c61e85596ddb31a79199dac`
- **Message (SHA-256 Hash):** `d32f7c1462e99983479c7d4319c0a3e85fe9acdba0c5c43a68f5efebb337d427`
- **Signature Hash:** `0x729a2038e6c9c2806458f2f7a1232b18b16ff421a8aeb93dd2bf5050da23e4fe354f803d7944bc49`

These records ensure permanent authorship traceability and satisfy open-science best practices for computationally generated research. Future versions will update the DOI and blockchain metadata but preserve this structure verbatim for continuity across publications.

Acknowledgments

We thank the maintainers of the NIST Atomic Spectra Database, as well as all open-data and research communities that make this work possible. We also thank colleagues and early

readers for constructive comments on clarity and falsification criteria. All remaining errors are the authors' own.

Publication Metadata

A Local Electromagnetic Wave Equation from Spectral Geometry.
DOI: 10.5281/zenodo.17402933
Version: 1.0 (First Edition)
Date: November 8, 2025

Related Works:

"Recursive Geometry of Atomic Spectra" — DOI: 10.5281/zenodo.17167686

"Information-Theoretic Confirmation of the α-Affine Thread Frame" — DOI: 10.5281/zenodo.17335814

"Systems and Methods for Photon-Only Motif Identification and Recursive Geometry Encoding (Photoncodes)" —
U.S. Provisional Patent Application No. 63/881,260, filed Sep. 13, 2025; USPTO Confirmation No. 8979 (Patent Center #72283661).

"Systems and Methods for Phonon-Based Recursive Geometry Encoding and Drift–Stability Analysis (Phononcodes)" —
U.S. Provisional Patent Application No. 63/893,959, filed Oct. 5, 2025; USPTO Confirmation No. 4939 (Patent Center #72586568).

"A System and Method for Encoding Electromagnetic Propagation on a Beta-Locked Lattice (Radiocodes)" —
U.S. Provisional Patent Application No. 63/914,041, filed Nov. 8, 2025; USPTO Confirmation No. 8105 (Patent Center #73095827).

Note. The referenced patent filings document the practical, machine-implemented encoding systems —*Photoncodes*, *Phononcodes*, and *Radiocodes*— that operationalize the theoretical framework developed here across photon, phonon, and electromagnetic domains. The present manuscript addresses only the underlying physical and mathematical theory; no claim of proprietary control over physical law is implied. In the engineering implementations, the slope parameter is treated as a predetermined implementation constant $\beta \approx \log_{10} \alpha$, consistent with the enablement language of the provisional applications.

Lucerna Veritas

Follow the light of the lantern.

References

Rissanen, Jorma (1978). "Modeling by Shortest Data Description". In: *Automatica* 14, pp. 465–471. DOI: 10.1016/0005-1098(78)90005-5.

Grünwald, Peter D. (2007). *The Minimum Description Length Principle*. Cambridge, MA: MIT Press.

Wheeler, John A. (1989). "Information, Physics, Quantum: The Search for Links". In: *Proceedings of the 3rd International Symposium on Foundations of Quantum Mechanics*. Tokyo: Physical Society of Japan.

Zurek, Wojciech H. (1989). "Algorithmic Randomness and Physical Entropy". In: *Physical Review A* 40.8, pp. 4731–4751. DOI: 10.1103/PhysRevA.40.4731.

Soklakov, Andrei N. (2002). "Occam's Razor as a Formal Basis for a Physical Theory". In: *Foundations of Physics Letters* 15.2. Applies Kolmogorov complexity and simplicity principles to derive classical mechanics., pp. 107–135. DOI: 10.1023/A:1015085832238.

Heaton, Kelly B. and CRC (2025a). "Recursive Geometry of Atomic Spectra". In: *Zenodo Preprint*. Introduces the α-Affine Thread Frame and slope $\beta = \log_{10}\alpha$. DOI: 10.5281/zenodo.17167686. URL: https://doi.org/10.5281/zenodo.17167686.

– (2025b). "Information-Theoretic Confirmation of the α-Affine Thread Frame: Minimum Description Length Validation of the Fine-Structure Slope". In: *Zenodo Preprint*. Applies the MDL principle to validate the fine-structure slope $\beta = \log_{10}\alpha$. DOI: 10.5281/zenodo.17335814. URL: https://doi.org/10.5281/zenodo.17335814.

Maxwell, James Clerk (1865). "A Dynamical Theory of the Electromagnetic Field". In: *Philosophical Transactions of the Royal Society of London* 155, pp. 459–512. DOI: 10.1098/rstl.1865.0008.

Grünwald, Peter D. and Teemu Roos (2019). "Minimum Description Length Revisited". In: *International Journal of Mathematics for Industry* 11.2, p. 1930001. DOI: 10.1142/S0218202519300014.

Kaluza, Theodor (1921). "Zum Unitätsproblem der Physik". In: *Sitzungsberichte der Preussischen Akademie der Wissenschaften, Mathematisch-Physikalische Klasse*. Introduces 5D unification; source-free Maxwell emerges from a cyclic extra coordinate., pp. 966–972.

Kobe, Donald H. (1980). "Derivation of Maxwell's Equations from the Gauge Invariance of Classical Mechanics". In: *American Journal of Physics* 48.5, pp. 348–353. DOI: 10.1119/1.12116.

Collins, Kristina, John Gibbons, David Kazdan, and Nathaniel Frissell (2024). *Grape V1 Data: Frequency Estimation and Amplitudes of North American Time Standard Stations*. Version 1.0. Dataset for the Earth System Science Data publication, covering PSWS Grape V1 frequency and amplitude measurements (2019–2020). Zenodo. DOI: 10.5281/zenodo.13637199. URL: https://doi.org/10.5281/zenodo.13637199.

Collins, Kristina, John Gibbons, Nathaniel Frissell, Aidan Montare, David Kazdan, Darren Kalmbach, David Swartz, Robert Benedict, Veronica Romanek, Rachel Boedicker, William Liles, William Engelke, David G. McGaw, James Farmer, Gary Mikitin, Joseph Hobart, George Kavanagh, and Shibaji Chakraborty (2023). "Crowdsourced Doppler measurements of time standard stations demonstrating ionospheric variability". In: *Earth System Science Data* 15. Open Access, Creative Commons Attribution 4.0 License, pp. 1403–1418. DOI: 10.5194/essd-15-1403-2023. URL: https://doi.org/10.5194/essd-15-1403-2023.

Hamilton, William Rowan (1834). "On a General Method in Dynamics". In: *Philosophical Transactions of the Royal Society of London* 124. Introduces the Hamiltonian formulation of mechanics., pp. 247–308. DOI: 10.1098/rstl.1834.0012.

Landau, Lev D. and Evgeny M. Lifshitz (1976). *Mechanics*. 3rd. Oxford: Pergamon Press.

Noether, Emmy (1971). "Invariant Variation Problems". In: *Transport Theory and Statistical Physics* 1.3. English translation of Noether's 1918 paper., pp. 186–207. DOI: 10.1080/00411457108231446.

Misner, Charles W., Kip S. Thorne, and John Archibald Wheeler (1973). *Gravitation*. See Chapter 25 for weak-field gravitational redshift. San Francisco: W. H. Freeman. ISBN: 978-0-7167-0344-0.

Carroll, Sean M. (2019). *Spacetime and Geometry: An Introduction to General Relativity*. 2nd. Section 5.1 for gravitational redshift in the weak-field limit. Cambridge: Cambridge University Press. ISBN: 978-1-108-48239-4.